FERMILAB-PUB-79-141-E E-396

COO-088-63

A Two-Jet Calorimeter Experiment At Fermilab

M. D. Corcoran[1], L. Cormell[2], M. Dris[2], A. R. Erwin[1], P. J. Gollon[3], A. Kanofsky[4], W. Kononenko[2], B. Robinson[2], W. Selove[2], M. Thompson[1], and B. Yost[2]

1. University of Wisconsin, Madison, Wisconsin 53706
2. University of Pennsylvania, Philadelphia, Pennsylvania 19104
3. Fermilab, Batavia, Illinois 60510
4. Lehigh University, Bethlehem, Pennsylvania 18015

13.85H Inelastic scattering, many-particle final states (energy > 10 GeV)

Abstract

A Two-Jet Calorimeter Experiment At Fermilab. M.D. Corcoran (Physics Department, University of Wisconsin, Madison Wisconsin 53706), L. Cormell, M. Dris, A.R. Erwin, P.J. Gollon, A. Kanofsky, W. Kononenko, B. Robinson, W. Selove, M. Thompson, and B. Yost.
Physica Scripta (Sweden).
A double arm calorimeter and drift chamber system has been used to study high P_T jets at Fermilab in 130, 200, and 400 GeV collisions with a hydrogen target. The response of the calorimeter to jets is discussed. Data are presented on the transverse momentum of partons in the pion and proton and on the pion structure function.

A Two-Jet Calorimeter Experiment At Fermilab

M. D. Corcoran[1], L. Cormell[2], M. Dris[2], A. R. Erwin[1], P. J. Gollon[3], A. Kanofsky[4], W. Kononenko[2], B. Robinson[2], W. Selove[2], M. Thompson[1], and B. Yost[2]

1. University of Wisconsin, Madison, Wisconsin 53706
2. University of Pennsylvania, Philadelphia, Pennsylvania 19104
3. Fermilab, Batavia, Illinois 60510
4. Lehigh University, Bethlehem, Pennsylvania 18015

Abstract

A double arm calorimeter and drift chamber system has been used to study high P_T jets at Fermilab in 130, 200, and 400 GeV collisions with a hydrogen target. The response of the calorimeter to jets is discussed. Data are presented on the transverse momentum of partons in the pion and proton and on the pion structure function.

1 Apparatus

The basic apparatus for this experiment is shown in figure 1 and is described in somewhat more detail elsewhere. [1] It is essentially a hydrogen target preceeded on either side by 24 absorption lengths of steel and concrete and followed by 6 planes of drift chambers and a double arm calorimeter. The construction of the two calorimeter arms is not exactly symmetrical about the beam as can be seen in figure 2. Running conditions were usually such that the left and right arm subtended about 1 1/2 and 2 steradians respectively in the center of mass.

2 Calorimeter Bias

The response of a calorimeter of this type to jet produced at hadron accelerators is not what one might have naively expected and thus deserves some discussion. In his original article suggesting jet studies [2] Bjorken pointed out that one would expect most detectors to miss about 1 GeV/c of the momentum in an average jet due to reasonable size limitations for calorimeters.

Calculations for our particular geometry fixed the expected loss to average about 800 MeV/c due to jet fragments outside the calorimeter acceptance. However, experimental evidence and more refined Monte Carlo calculations show that we tend to measure the correct momentum for those jets which we do detect.

This surprising result was first suggested to us by M. Dris. [3] The single most important factor contributing to this effect is the steep p_T dependance of the jet cross sections

in the Fermilab energy range, $d\sigma/dp_T \propto \exp(-3p_T)$ to $\exp(-4p_T)$. One must couple this with the large probability that for some jets all the jet fragments will be captured by our calorimeter. This probability is about 20% if hadron jets have a flat rapidity distribution as seems to be true of SPEAR jets. [4] Now one has only to ask, "If the calorimeter measures 5 GeV/c, is it more likely that it has seen a 6 GeV/c jet which has lost 1 GeV/c of fragments or is it more likely that it has seen a 5 GeV/c jet with all of its fragments collected?" Since 6 GeV/c jets are about 30 times less probable than 5 GeV/c jets and about 20% of 5 GeV/c jets are completely collected, this event is more likely to be a 5 GeV/c jet which registered correctly as 5 GeV in the calorimeter. Monte Carlo calculations, which also take into account less important angle and momentum resolution effects, show that on the average the calorimeter gives almost exactly the correct momentum for any jet that it detects.

A corollary to the Dris theorem just discussed would say that the spatial size and multiplicity of the jet detected is defined by the size of the triggering calorimeter. Indeed this appears to be true. If we trigger in software using a subset of calorimeter segments in the center of the right arm with only 1/2 the solid angle of the whole right arm, then we obtain a sample of jets with almost all of the energy contained in the solid angle used for triggering, the remainder of the calorimeter having very little energy, most of which can be attributed to lateral shower development from the triggering

segments. Refer to figure 3. Thus a calorimeter can be expected to give the correct momentum for the jets it records, but it will necessarily not give the correct cross section because of the unrecorded jets whose size was too large for the calorimeter.

Another corollary which may seem useful later, is that calorimeters may preferentially detect quark jets over gluon jets. Since one may think of a gluon as breaking into a quark-antiquark pair, it seems likely that gluon jets will be spatially more diffuse and have about twice the multiplicity together with correspondingly smaller momentum fragments.

3 Transverse Momentum Balance

When one triggers on a p_T deposited in the left arm, there appears to be a tendency for a nearly balancing p_T to appear in the right arm, and in almost no case is there a failure to find at least some compensating p_T in the arm away from the trigger side. See figures 4 and 5. This is in contrast to all other reported jet experiments to date. Most other experiments impose some restriction on total collection of energy on the away side, either by a magnetic field, by failure to collect neutrons and K_L^o's or by using cuts which restrict accumulation of small contributions.

Peripheral phase space calculations show that this degree of p_T balance in the solid angle of our apparatus would not be expected for ordinary events until final state multiplicities of 25 particles or more. See figure 6. One may guess the cross section for such high multiplicities using bubble chamber data,

and it is almost comparable to the observed calorimeter cross sections. However, the multiplicities of the phase space jets are almost twice as large as those of the calorimeter jets as compared in figure 7.

A double arm trigger in this experiment is effected by requiring that the scalar hardware sum of p_T in the left and right arm be greater than some threshold. A scatterplot of p_T (LEFT) vs. p_T (RIGHT) is given in figure 8 and shows a preference for balanced p_T. The peaking along the diagonal is much sharper than one can discern from the scatter plot. This is shown in figure 9 by plotting the distribution of points along a cut perpendicular to the diagonal. The width of this distribution is much larger than the momentum resolution of the calorimeter and must be attributed to physical effects such as the transverse momentum of the partons.

The transverse momentum of the partons is most accurately studied by looking at the vector sum of $\underset{\sim}{p_T}$ (LEFT) + $\underset{\sim}{p_T}$ (RIGHT)= $\underset{\sim}{K_T}$. This should be zero in the absence of any initial transverse momentum provided we have collected all final state momentum. The y-component of this vector is somewhat limited by the angular aperture of the calorimeters, but the x-component may assume any value. We have therefore plotted the root mean square of K_{Tx} with the upper points in figure 10. The lower points are the same value of K_{Tx} from a Monte Carlo program that includes p_T dependence of the cross section and the angular and momentum resolution of the calorimeters.

The points of figure 10 are for 400 GeV p-p collisions. After subracting the instrumental broadening computed by the Monte Carlo program we find K_{Tx} (R.M.S.) $\cong$ 1.2 GeV/c. By virtue of the quadratic combination of the transverse momentum fluctuations of quarks one and two, this number is also the root mean square transverse momentum of one quark.

$$K_{Tx}^2 = K_{1x}^2 + K_{2x}^2 = K_{1x}^2 + K_{1y}^2 = K_1^2$$

The value of K_{Tx} (R.M.S.) is the same for πp and p-p collisions at a given energy. It does seem to increase linearly with center of mass energy as $\sqrt{s}$. There appears to be a residual value of K_{Tx} (R.M.S.) at $\sqrt{s} = 0$ in the neighborhood of 600 MeV/c.

4 π-p and p-p Differences

From the simple notion that pions are made of a quark-antiquark pair and that protons are made of 3 quarks one can predict a correlation for jet pairs that will differ in πp and pp collisions. Figure 11 shows average πp and pp collisions involving valence quark constituents. Since on the average pion quarks carry a larger fraction of the hadron momentum than proton quarks, both members of the jet pair from πp collisions should tend to go forward more frequently in πp collisions than in pp collisions. This can be checked in a way that is independent of absolute cross section measurements by studying the ratio of the number of pp events to πp events at different center of mass angles, θ_L^* and θ_R^*, for the two jets

Figure 12 is a summary of such a study. [1] Briefly one can see that the ratio of pp induced jets to πp induced jets is different by more than a factor of 3 when we compare jets which are both at 90° in the cms to those which are both at 60° in the cms.

This last result suggests that one might be able to obtain the structure function for quarks in the pion. Since our apparatus does not distinguish charge, there is no possibility of distinguishing the quark or antiquark jet after the collision. In any case we will assume the structure function $f_{(q+\bar{q}),\pi}(x)$ to be the same for these two pion constituents. If the apparatus discriminates against gluons, as we speculated earlier, we may assume in addition that we are not observing gluon-gluon or quark-gluon collisions. By ignoring any distinctions among parton species we may write the ratio of p-p to π-p cross sections as

$$\frac{\sigma_p}{\sigma_\pi} = \frac{f_p(x_1)\ f_p(x_2)\ \ d\sigma/dt'\ (s',\ t')}{f_\pi(x_1)\ f_p(x_2)\ \ d\sigma/dt'\ (s',\ t')}$$

where $x = 2p_L/\sqrt{s}$, $f_\pi(x)$ is the pion structure function, and s' and t' are the energy squared and 4-momentum transfer squared in the quark-quark scattering. Values for the proton structure function $f_p(x)$ have been determined from deep inelastic ep scattering. We take our values for $f_p(x)$ as those used by Field and Feynman. [5]

The resulting structure function for the pion is given as a function of x in figure 13. Since it involves only the ratio of pp and πp induced events, it requires no overall normalization. The dashed curve in figure 13 is an older theoretical prediction of G. Farrar [6] and the solid curve is a more recent prediction of Field and Feynman. [5]

If the factorization we have assumed in this analysis is valid, then the results should be independent of s', t', and the x_2 of the target proton. Within our statistical errors this is easily true. Although it is smaller than the statistical errors, there does appear to be some slight systematic difference between data points obtainted at 200 GeV/c and 130 GeV/c beam momentum. The difference is in such a direction that it may be accounted for by the non-scaling behavior of the proton structure function. We did not attempt to exploit such behavior in this analysis.

References

1. A. R. Erwin, New Results in High Energy Physics - 1978 Vanderbilt Conference, R. S. Panvini and S. E. Csorna editors, p.64, American Institute of Physics, New York 1978. M. D. Corcoran et al., Phys. Rev. Lett. 41, 9 (1978).
2. J. D. Bjorken, Phys. Rev. D8, 4098 (1973).
3. Manolis A. Dris Jet Bias Effect due to Small Detector Size, accepted for publication in Nuclear Instruments and Methods, 1978.
4. Gail G. Hanson, SLAC Preprint, SLAC-PUB-2118, May 1978.
5. R. D. Field and R. P. Feynman, Phys. Rev. D15, 2590 (1977).
6. Glenys R. Farrar, Nucl. Phys. B77, 429 (1974).

Figure Captions

Figure 1. Schematic floor plan of the experimental apparatus.

Figure 2. The two calorimeter arms as seen from the target.

Figure 3. Upper histograms refer to p_T and multiplicity distributions for events that deposit 4 GeV/c in the "inner" 0.8 sr. of the right calorimeter arm. Lower histograms show the p_T and multiplicity distributions for the same events in the surrounding "outer" 1.3 sr. of the right arm.

Figure 4. P_T spectrum for the calorimeter on the away side (inverted histogram) when the calorimeter on the trigger side has p_T in the bins shown (erect histogram).

Figure 5. Relation between peak p_T on the away side to trigger p_T (solid curve). Three points generated by a 15 body phase space program illustrate the small extent to which p_T conservation forces particles into the away side at these values of x_T.

Figure 6. Response of the calorimeters to 25 body events generated by invariant phase space times $\exp(-6p_T)$ when the right arm threshold is set at $p_T = 1.5$ GeV/c.

Figure 7. Solid histogram shows multiplicity distribution, charged plus neutral, for jets whose momentum vector centered in the right arm and which have $p_T > 3.5$ GeV. The multiplicity algorithm requires at least

segment of the calorimeter near the particle hit site to have $p_T > 0.3$ GeV/c. Dashed histogram shows a higher multiplicity for 25 body phase space events with total $p_T > 1.5$ GeV/c

Figure 8. Scatterplot of p_T in the left and right arm for double arm triggers at 400 GeV/c.

Figure 9. Solid Curve: True density of events in figure 8 along a direction y' which is perpendicular to the diagonal x' in the scatterplot. Increasing x' represents increasing p_T for the scatter. Dashed Curve: Density of Monte Carlo events when each arm has an independent p_T spectrum satisfying previous single arm spectrometer experiments.

Figure 10. The root mean square fluctuation of the x-component of the transverse momentum unbalance for the two jets at 400 GeV/c beam momentum. Upper points are data. Lower points show fluctuation expected due to finite acceptance, momentum resolution and discrete angle resolution of the detectors.

Figure 11. Naive picture showing why parton structure functions tend to make both jets go forward in the πp center of mass system.

Figure 12. Ratio of the number of pp to πp produced jets as a function of cms angles in double arm triggers at 130 GeV/c. The p_T of an event in this plot was between 2.5 and 2.75 GeV/c where $p_T = (p_T\ (\mathrm{LEFT}) + p_T\ (\mathrm{RIGHT}))/\ 2.0$.

Figure 13. Average structure function for the quark and antiquark in a pion obtained from two jet final states. Curves are theoretical predictions.

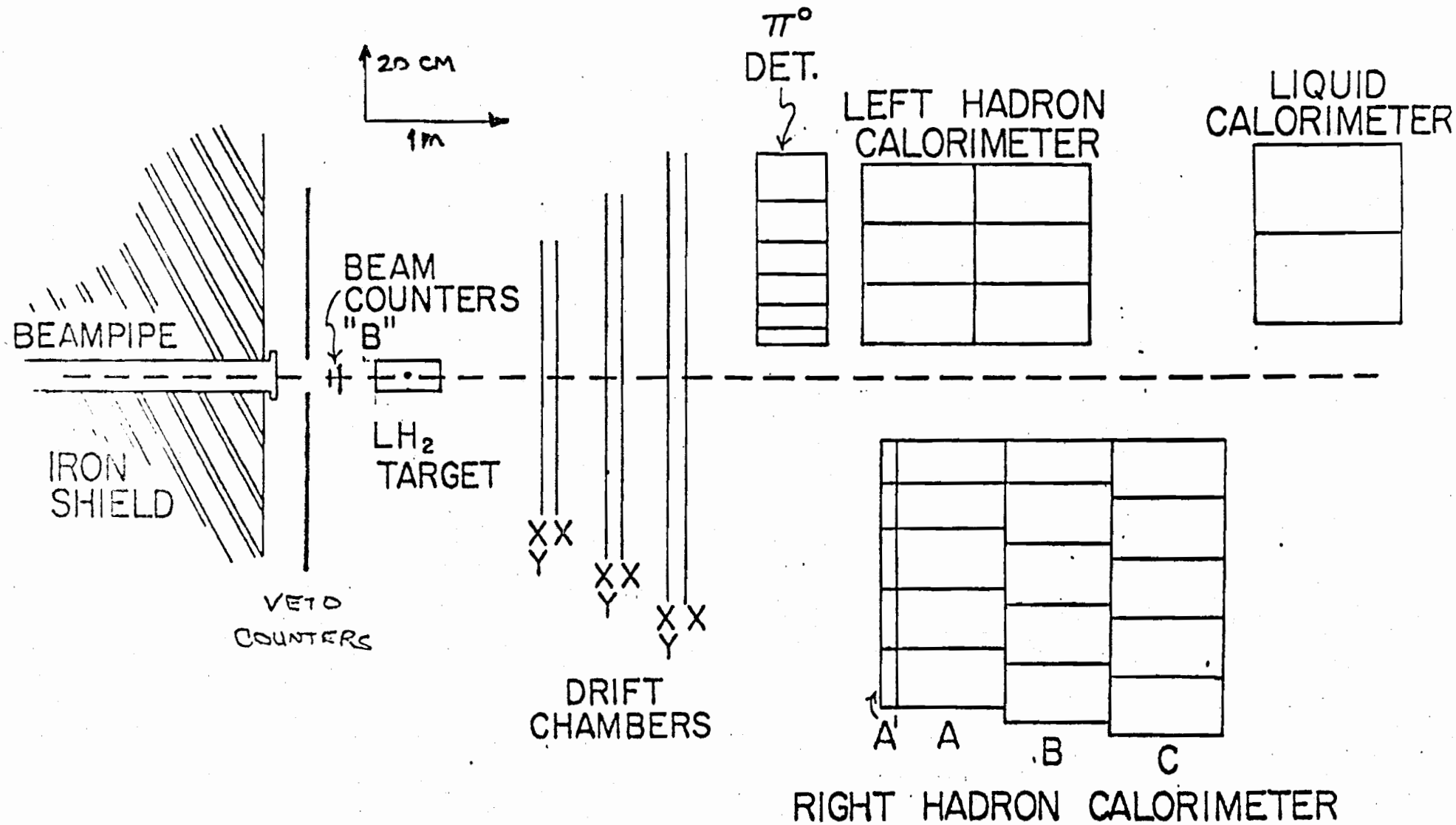
20 CM
1m
BEAMPIPE
IRON SHIELD
VETO COUNTERS
BEAM COUNTERS "B"
LH2 TARGET
X X
Y
X X
Y
X X
Y
DRIFT CHAMBERS
π°
DET.
LEFT HADRON CALORIMETER
LIQUID CALORIMETER
A'
A
B
C
RIGHT HADRON CALORIMETER

Figure 1

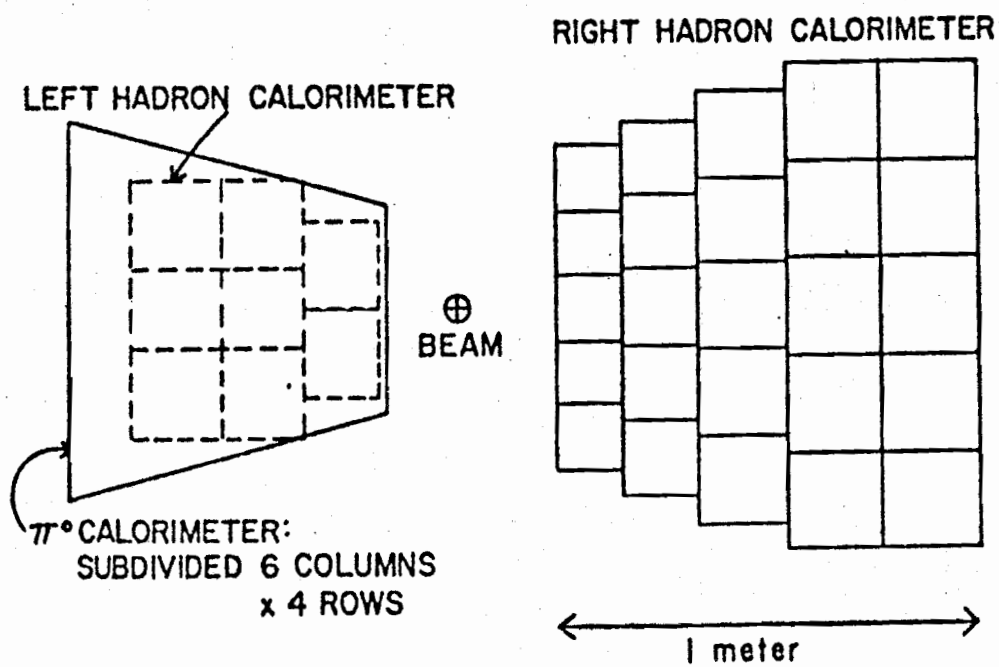
RIGHT HADRON CALORIMETER
LEFT HADRON CALORIMETER
⊕
BEAM
π° CALORIMETER:
SUBDIVIDED 6 COLUMNS
x 4 ROWS
1 meter

Figure 2

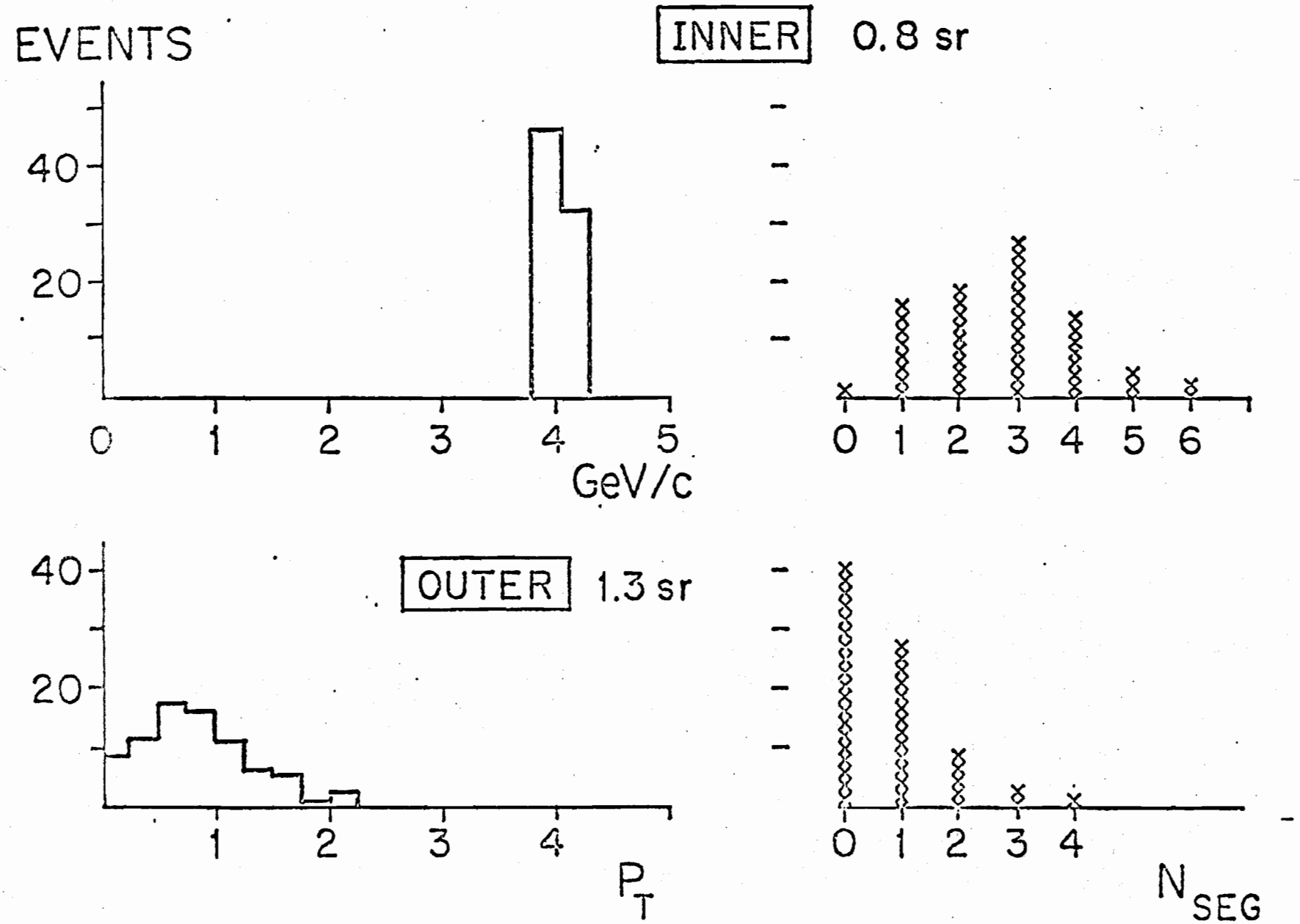
EVENTS
INNER
0.8 sr
40
20
0
1
2
3
4
5
GeV/c
0
1
2
3
4
5
6
OUTER
1.3 sr
40
20
1
2
3
4
P_T
0
1
2
3
4
N_{SEG}

Figure 3

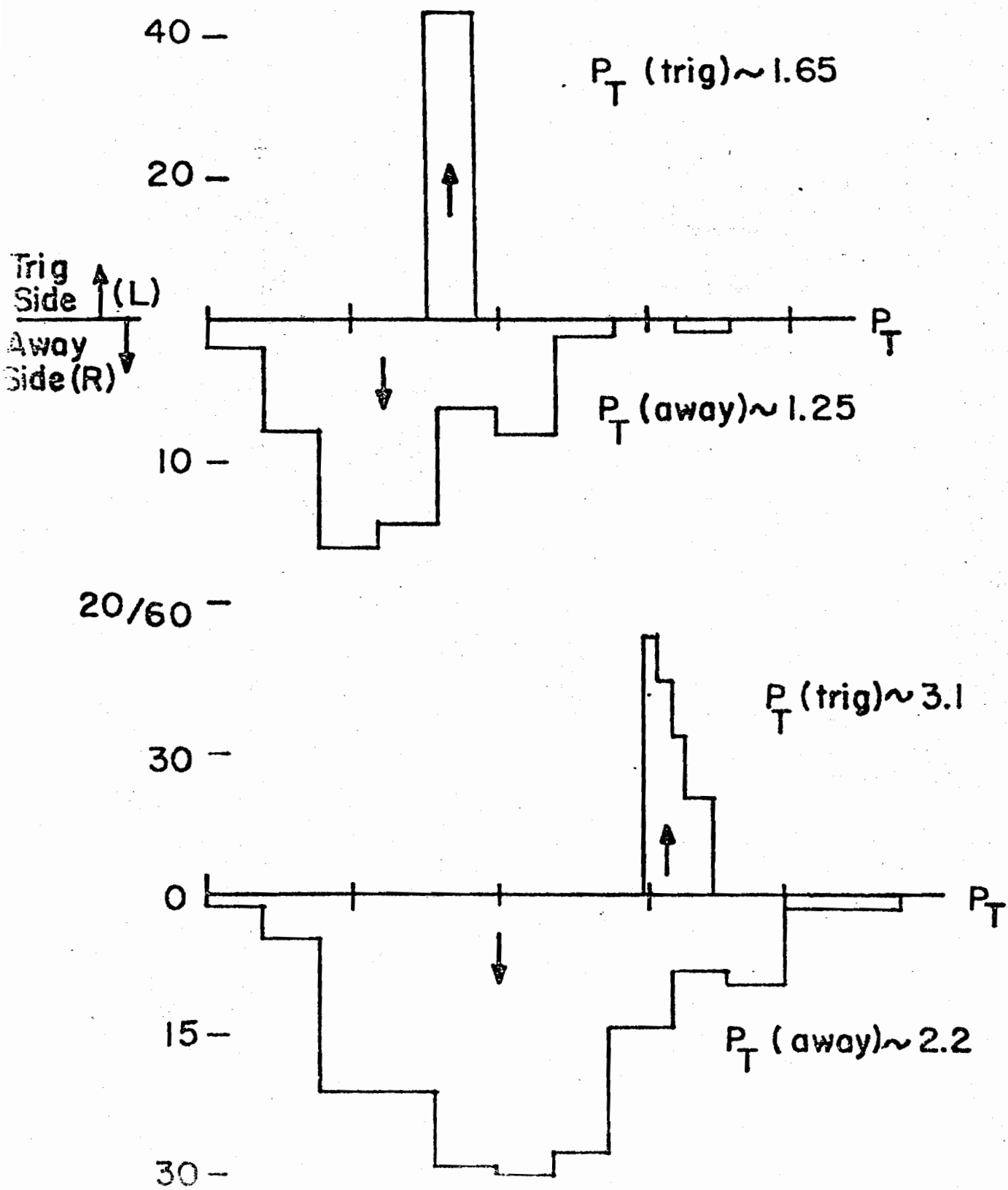

The Away-Side P_T Spectrum for Two P_T (trig) Bands

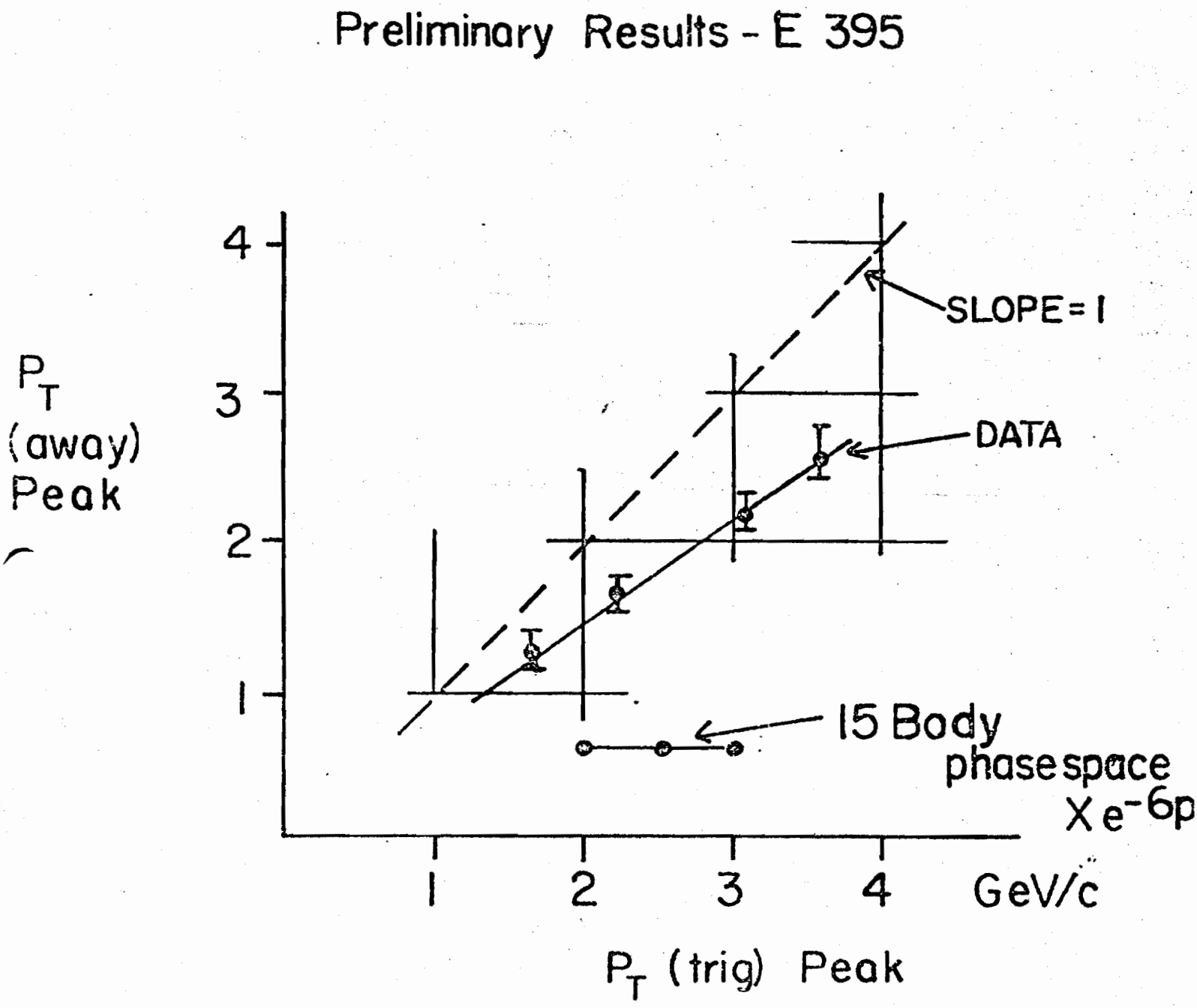
Preliminary Results - E 395
P_T (away) Peak
4
3
2
1
SLOPE = 1
DATA
15 Body phase space X e^{-6p}
1
2
3
4
GeV/c
P_T (trig) Peak

Figure 5

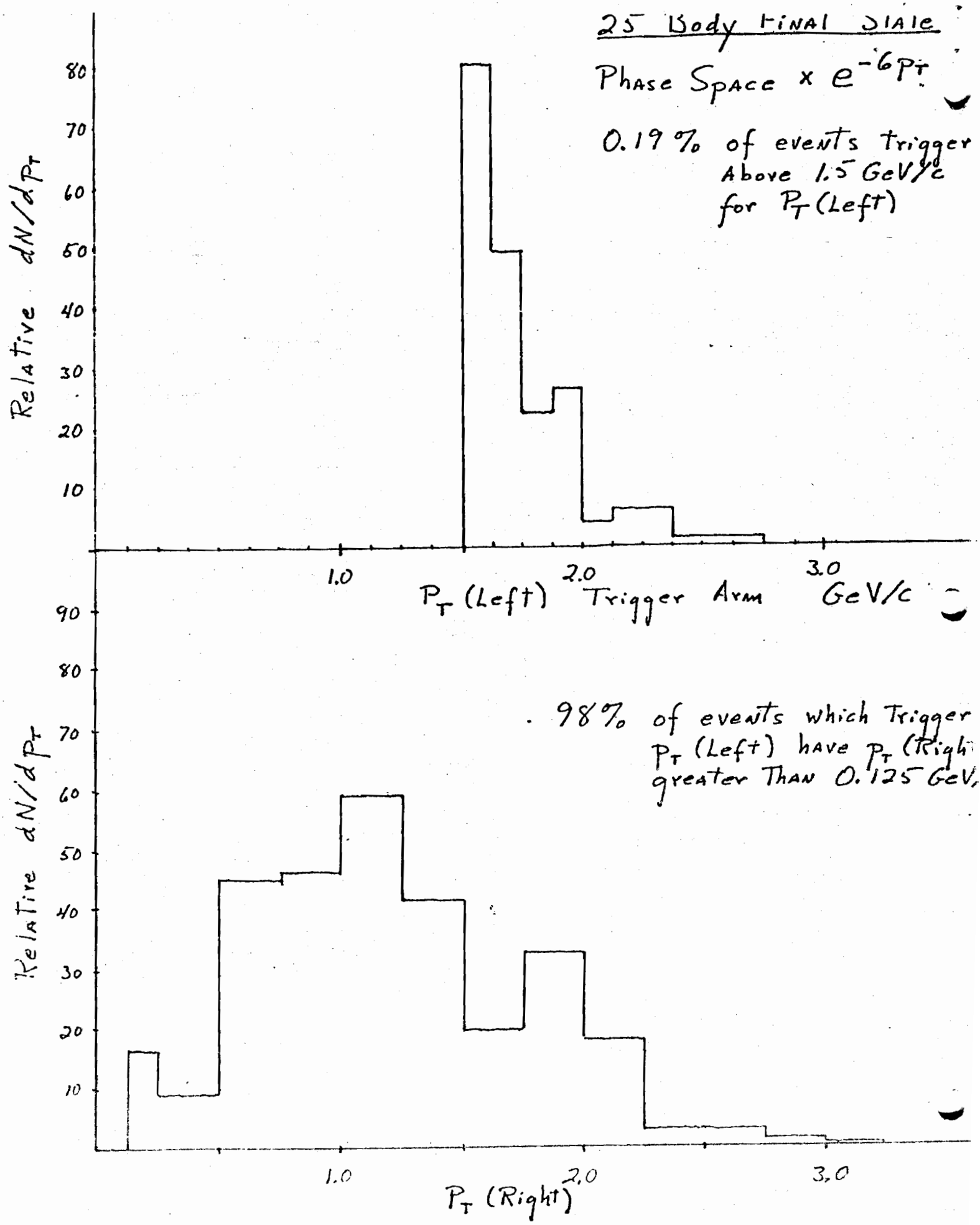
25 Body Final State
Phase Space x e^{-6P_T}
0.19% of events trigger Above 1.5 GeV/c for P_T (Left)
Relative dN/dPT
80
70
60
50
40
30
20
10
1.0
2.0
3.0
P_T (Left) Trigger Arm GeV/c
98% of events which Trigger P_T (Left) have P_T (Righ greater Than 0.125 GeV,
Relative dN/dPT
90
80
70
60
50
40
30
20
10
1.0
2.0
3.0
P_T (Right)

Figure 6

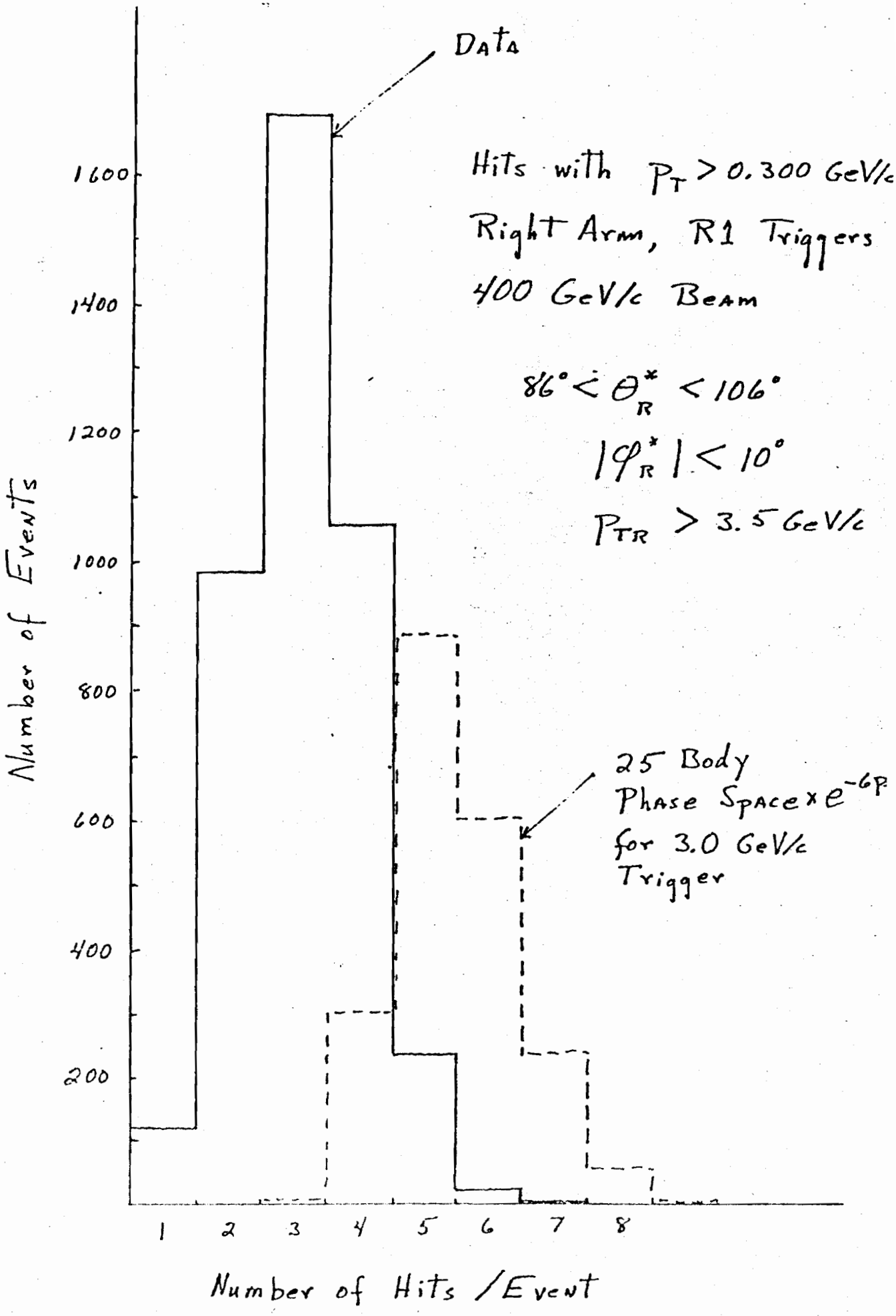
Data
Hits with $p_T > 0.300$ GeV/c
Right Arm, R1 Triggers
400 GeV/c Beam
$86° < \theta_R^* < 106°$
$|\varphi_R^*| < 10°$
$p_{TR} > 3.5$ GeV/c
25 Body
Phase Space $\times e^{-6p}$
for 3.0 GeV/c
Trigger
Number of Events
1600
1400
1200
1000
800
600
400
200
1
2
3
4
5
6
7
8
Number of Hits / Event

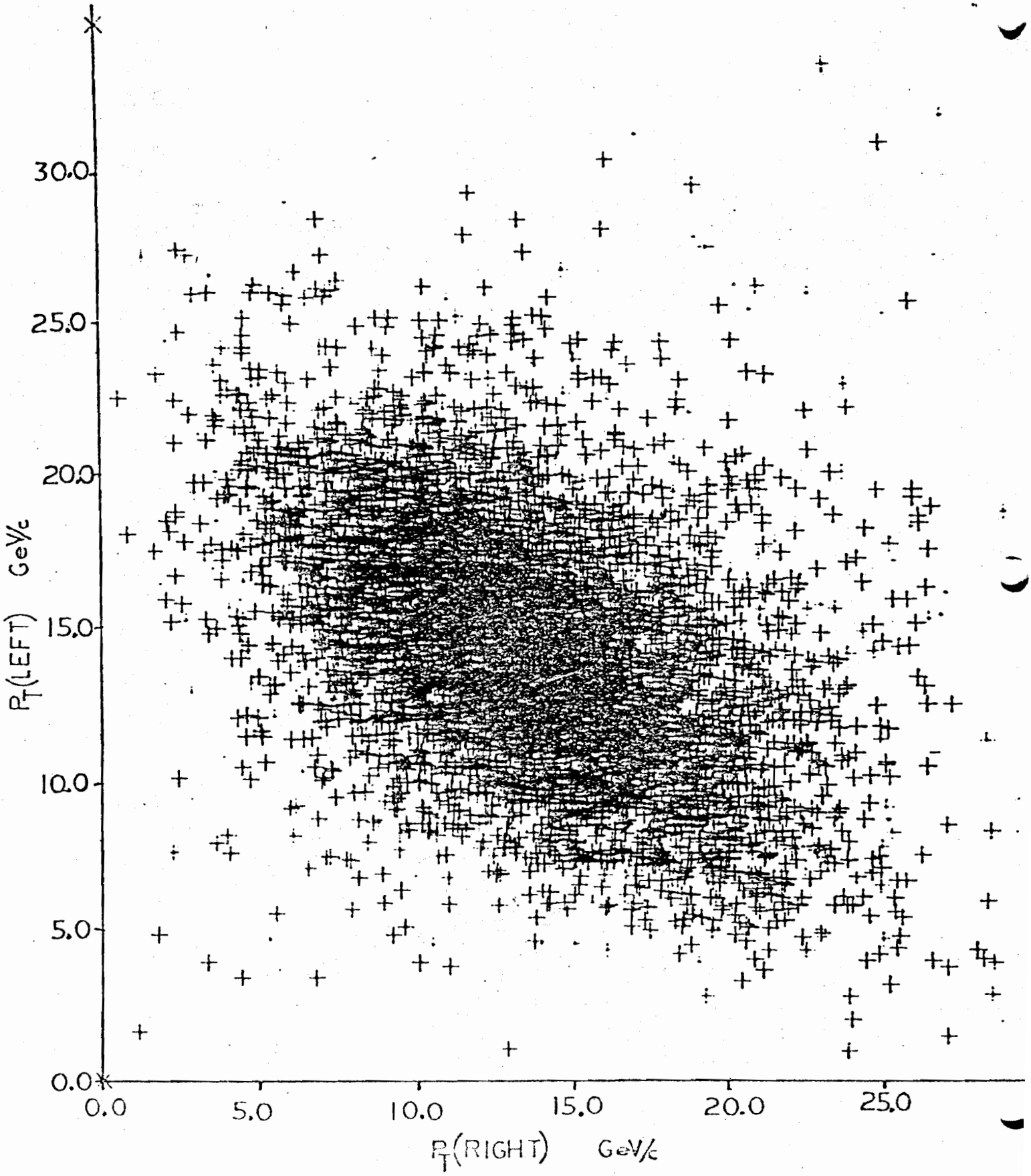
30.0
25.0
20.0
15.0
10.0
5.0
0.0
P_T(LEFT) GeV/c
0.0
5.0
10.0
15.0
20.0
25.0
P_T(RIGHT) GeV/c

Figure 8

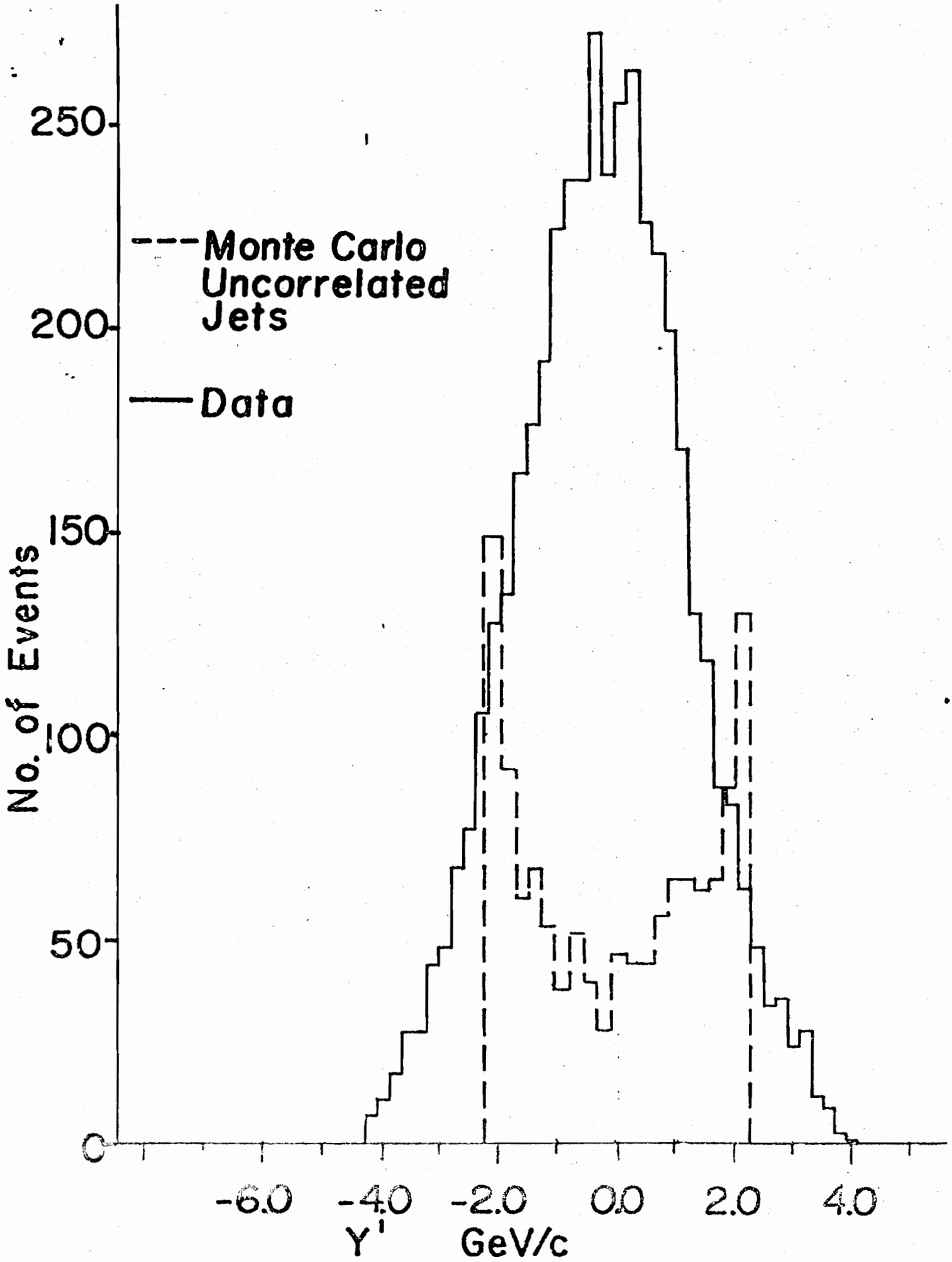
Monte Carlo Uncorrelated Jets
Data
No. of Events
250
200
150
100
50
0
-6.0
-4.0
-2.0
0.0
2.0
4.0
Y'
GeV/c

Figure 9

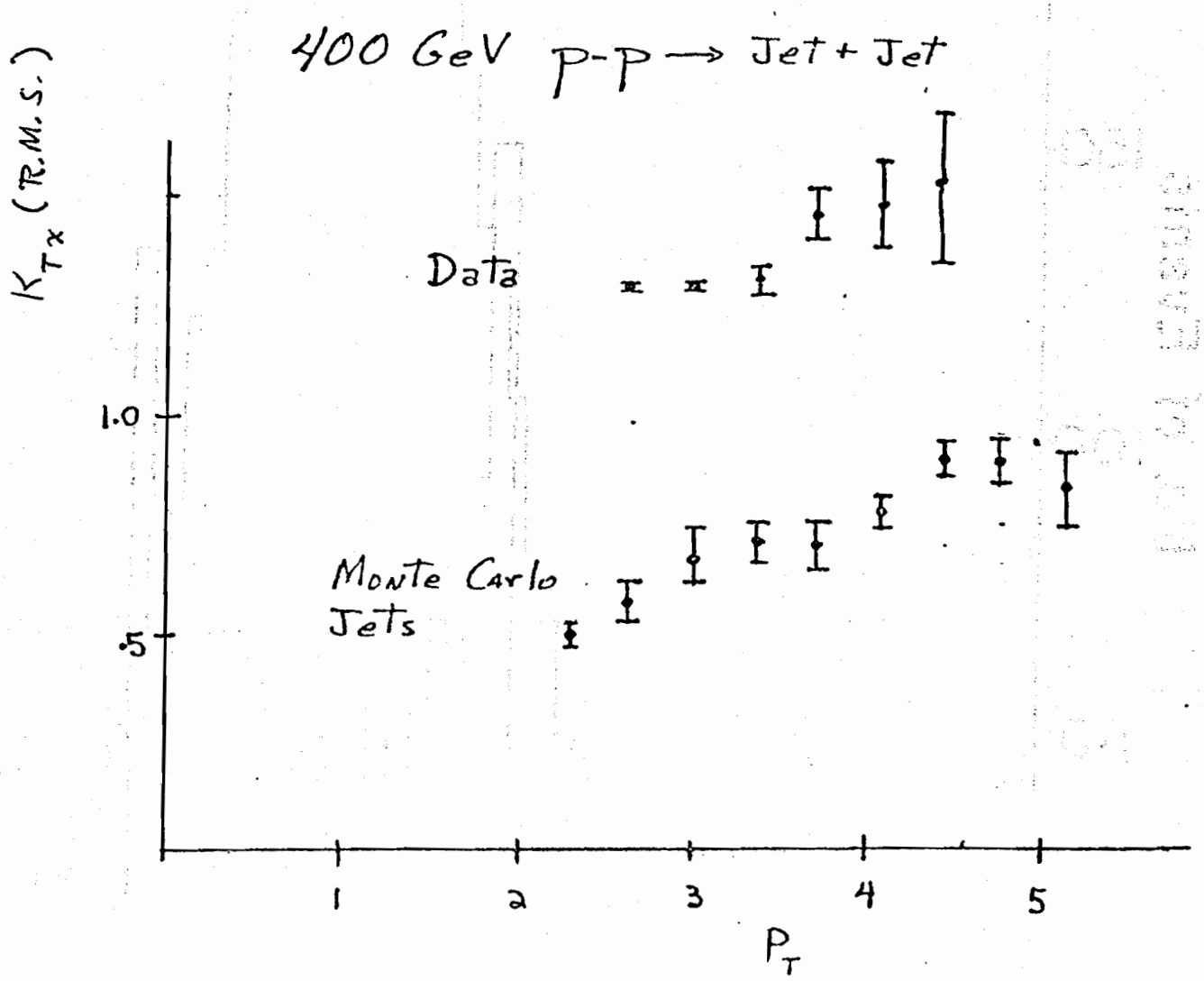

Figure 10

In Overall C.M.S.

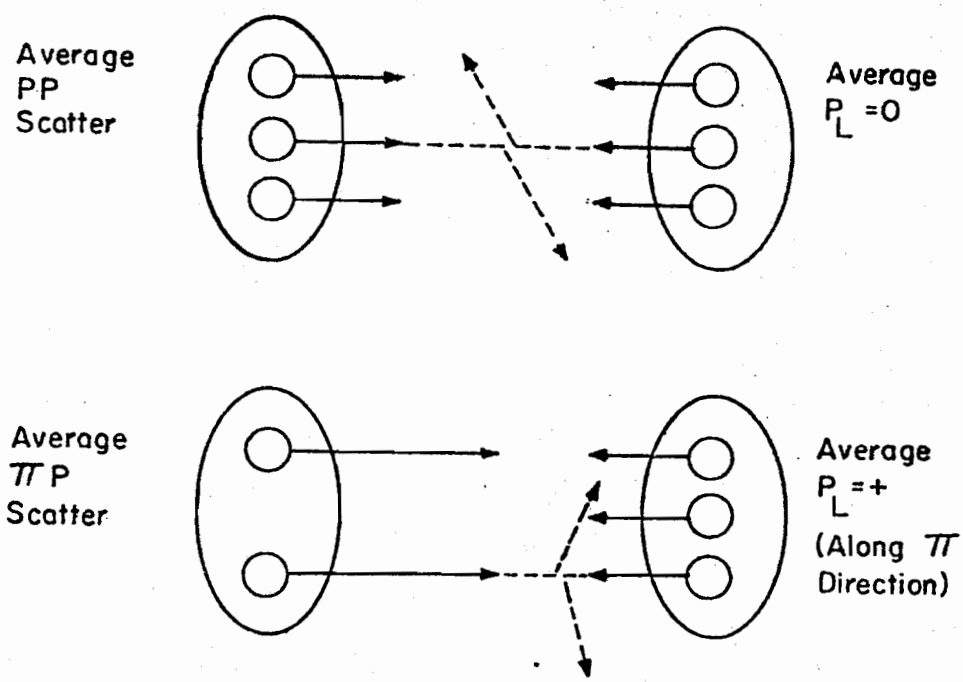

In the Overall C.M.S. one should find both jets in the forward hemisphere more frequently in πP collisions than in the PP collisions.

So plot

$$R(\theta_L^*, \theta_R^*) = \frac{\sigma(PP \rightarrow Jets)}{\sigma(\pi P \rightarrow Jets)}$$

Use P_T large enough to get angle definition in the C.M.S.

Figure 11

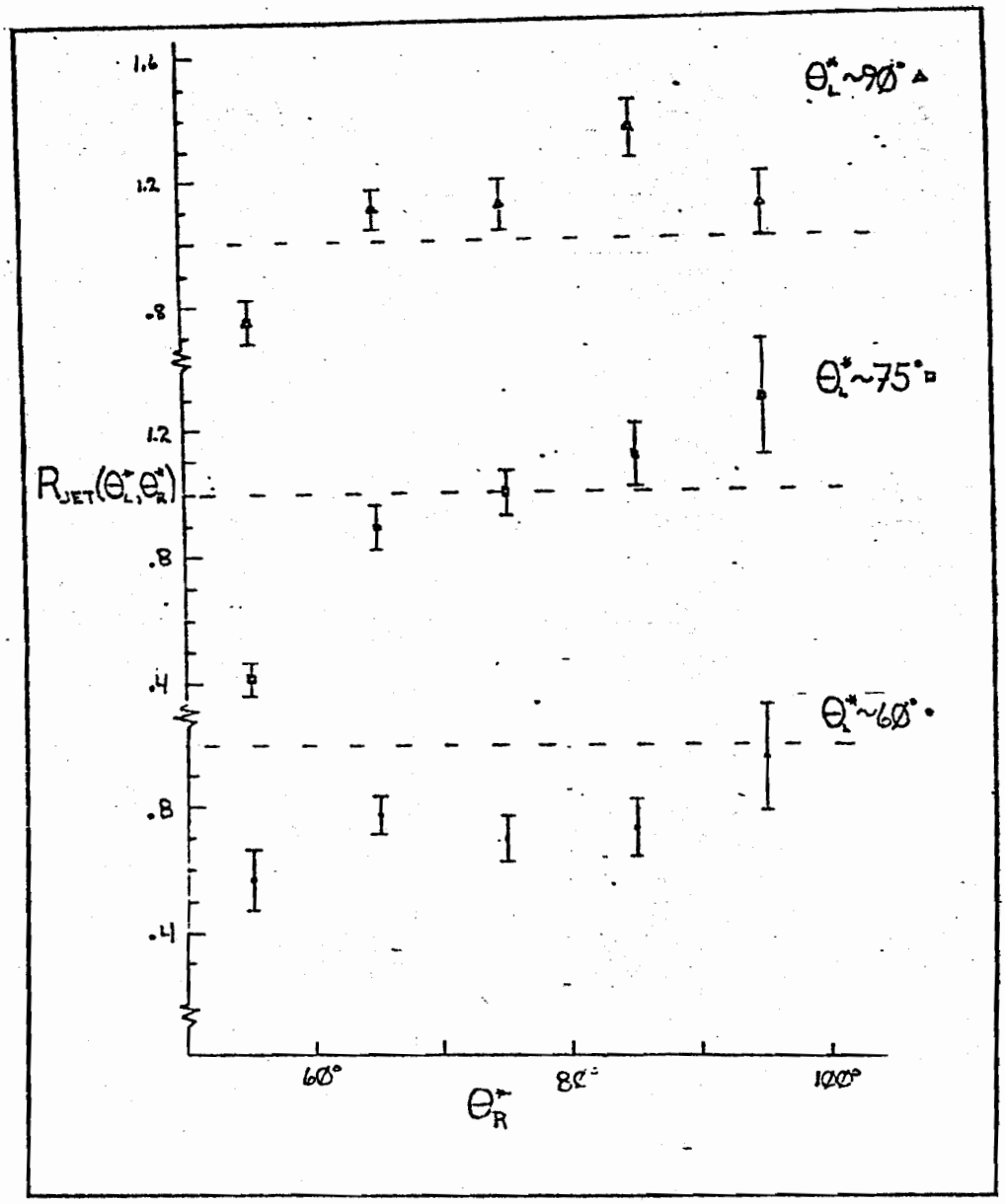
1.6
1.2
.8
1.2
.8
.4
.8
.4
$R_{JET}(\theta^*_L, \theta^*_R)$
$\theta^*_L \sim 90°$
$\theta^*_L \sim 75°$
$\theta^*_L \sim 60°$
60°
80°
100°
θ^*_R

Figure 12

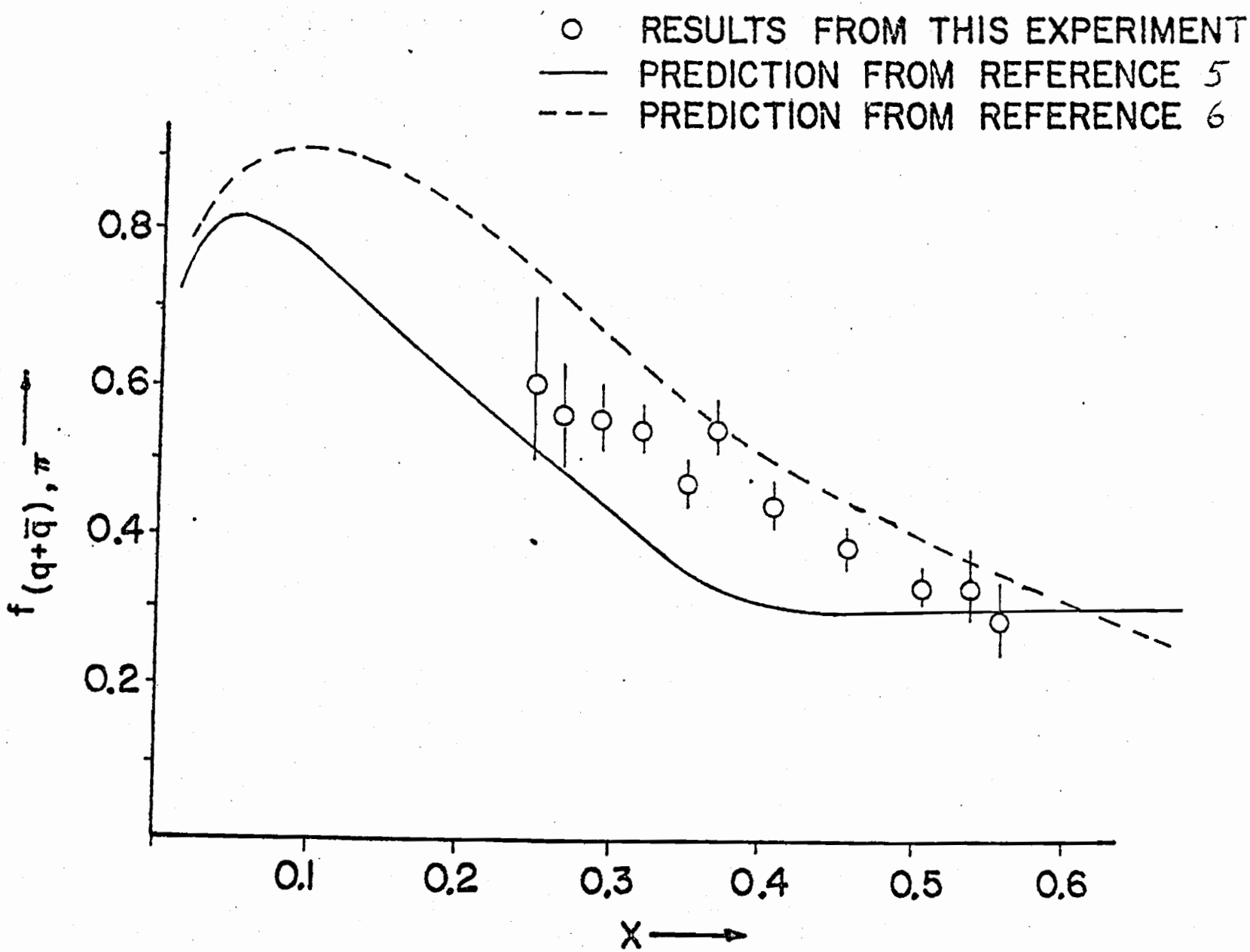
RESULTS FROM THIS EXPERIMENT
PREDICTION FROM REFERENCE 5
PREDICTION FROM REFERENCE 6
0.8
0.6
0.4
0.2
$f_{(q+\bar{q}),\pi^-}$
0.1
0.2
0.3
0.4
0.5
0.6
X

Figure 13